THE JOURNAL OF PHYSICAL CHEMISTRY C

Article

Cite This: J. Phys. Chem. C 2018, 122, 29249−29258

pubs.acs.org/JPCC

Crystal Facet Dependence for the Selectivity of C_2 Species over Co_2C Catalysts in the Fischer−Tropsch Synthesis

Baojun Wang, Danli Liang, Riguang Zhang,* and Lixia Ling

Key Laboratory of Coal Science and Technology of Ministry of Education and Shanxi Province, Taiyuan University of Technology, Taiyuan 030024 Shanxi, P. R. China

Supporting Information

ABSTRACT: The effect of Co_2C crystal facets on the selectivity of C_2 species (C_2 oxygenates and hydrocarbons) in Fischer−Tropsch synthesis (FTS) reaction was investigated using density functional theory calculations, and the selectivity comparisons among five exposed Co-termination (101), (011), (010), (110), and (111) crystal facets are examined to shed light on the essential relationship between FTS selectivity and the structure of Co_2C crystal facets. The results show that the C−C bond of C_2 species prefers to be formed instead of C_1 species CH_4 over Co_2C catalysts in the FTS reaction, and the selectivity of C_2 species and the dominant existence form of key CH_x intermediates are sensitive to the crystal facet of Co_2C catalysts, which are closely associated with Co_2C crystal facet's electronic and structural properties. The electronic and structural properties of different Co_2C crystal facets show that the high selectivity of C_2 oxygenates over the (011) and (111) facets are attributed to the upshift of their surface d-band centers, as well as the presence of the step B_5-type active unit with five Co atoms consisted of much denser surface active sites. However, both (101) and (010) facets exhibit high selectivity toward C_2 hydrocarbons, and the (110) facet presents high selectivity toward the formation of CH_4. Thus, regulating the exposed crystal facets of Co_2C catalyst can control the selectivity of desirable C_2 species. This work provides evidence at a molecular level to support that the sensitivity of Co_2C crystal facet is a cause to affect the selectivity of desired products in the FTS reaction.

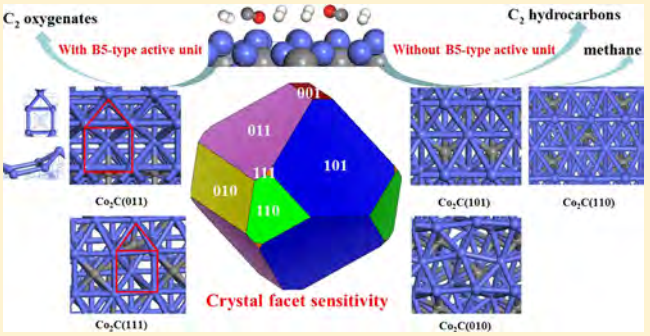

1. INTRODUCTION

Co_2C catalysts have been widely used in Fischer−Tropsch synthesis (FTS) to form olefins,[1] higher alcohols,[2−4] and aldehydes.[5] Meanwhile, the presence of bulk Co_2C is closely associated with metal promoter, for example, K[5] or La[6−9] promotes the formation of bulk Co_2C phase, and Co_2C quadrangular nanoprisms are formed with the addition of Mn[1] or Na.[10] Thus, the presence of Co_2C was favorable and stable in the FTS reaction with the help of metal promoters.

It is well known that Co_2C can contribute to the synthesis of C_2−C_4 olefins and higher alcohols in the FTS reaction; Zhong et al.[1,10] experimentally synthesized Co_2C nanoprisms with the dominantly exposed (101) crystal facet, which favors the production of lower olefins and inhibits CH_4 formation. On the contrary, previous experiments proved that Co_2C plays an important role in the synthesis of higher alcohols; Volkova et al.[11] found that Co_2C can activate CO and help CO insertion into carbonaceous species to form higher alcohols in the FTS at around 500 K. Fang et al.[7,8] prepared the Co−Cu bimetallic catalyst supported on $LaFeO_3$ or $La_2O_2CO_3$, which exhibits high activity and selectivity toward higher alcohols due to the presence of Co_2C at around 555 K. Jiao et al.,[6] Pei et al.,[12,13] and Du et al.[14] obtained the same experimental results that Co_2C is in favor of the synthesis of higher alcohols in the FTS reaction. Our recent density functional theory (DFT) studies about the selectivity of FTS reaction over different Co_2C crystal facets[3] show that the (111) facet exhibits an unexpectedly high selectivity toward the formation of C_2 oxygenates, whereas the (101) and (110) facets present a high selectivity toward the formation of C_2 hydrocarbons. Thus, two types of different views exist for the role of Co_2C active phase, one is for the formation of lower olefin, and the other is for the formation of higher alcohol. On the other hand, previous experimental and theoretical studies[1,5,10,15−17] have shown that the Co_2C(101), (011), (010), (110), and (111) low index surfaces can be exposed, and the corresponding surface area proportions based on the Wulff construction are 40.72, 35.21, 11.80, 9.87, and 0.27%, respectively.[17] Further, previous studies[15−17] have experimentally and theoretically showed that different CO/H_2 ratios affect the exposed termination of Co_2C catalyst in FTS reactions and the C-terminated Co_2C surface is mainly exposed in the CO-rich atmosphere, whereas the Co-terminated surface is dominantly exposed in the hydrogen-rich atmosphere. Because the FTS

Received: September 7, 2018
Revised: November 27, 2018
Published: November 29, 2018

DOI: 10.1021/acs.jpcc.8b08783
J. Phys. Chem. C 2018, 122, 29249−29258

reactions usually occurred in the hydrogen-rich condition, the Co-terminated Co_2C crystal facets represent a typical structure of Co_2C catalyst.[15,16]

As mentioned above, although the effect of the Co_2C crystal facet on the selectivity of C_2 species in the FTS reaction has been experimentally and theoretically investigated over the Co-terminated $Co_2C(101)$, (110), (111), and (020) crystal facets,[1,3] the selectivity of C_2 species over the Co-terminated $Co_2C(011)$ and (010) crystal facets with the corresponding surface area proportion of 35.21 and 11.80% is still unknown. As a result, given to the lack of the information over Co-terminated $Co_2C(011)$ and (010) with the total surface area proportion of 47.01%, the comparisons of C_2 species selectivity in the FTS reaction among the most exposed $Co_2C(101)$, (011), (010), (110), and (111) surfaces cannot be carried out, and the structure−selectivity relationship between FTS selectivity and Co_2C crystal facet is still unclear. Hence, there is plenty of space for researchers to understand FTS selectivity over the Co-terminated $Co_2C(011)$ and (010) surfaces and identify the corresponding FTS product distribution. More importantly, the C_2 species selectivity of the FTS reaction among the most exposed $Co_2C(101)$, (011), (010), (110), and (111) surfaces are compared to obtain the structure−selectivity relationship between FTS selectivity and Co_2C crystal facets.

This study is designed to investigate the formation mechanism of C_2 species in the FTS reaction over the Co-terminated $Co_2C(010)$ and (011) crystal facets to identify the effect of Co_2C crystal facets on the FTS selectivity. More importantly, on the basis of the information of $Co_2C(010)$ and (011) surfaces, taking the FTS selectivity over the most exposed $Co_2C(101)$, (011), (010), (110), and (111) surfaces into consideration, the structural and electronic properties of these crystal facets are identified to obtain the intrinsic relationship between FTS selectivity and the structure of Co_2C crystal facets. Further, the achieved insights can provide a theoretical clue for the design of high-performance Co_2C catalysts toward the desired products in the FTS reaction.

2. COMPUTATIONAL MODELS AND METHODS

The Co-terminated $p(2 \times 3)$ $Co_2C(010)$ and $p(3 \times 1)$ $Co_2C(011)$ surfaces with a 15 Å vacuum layer are employed in this study. As shown in Figure 1, for the $Co_2C(010)$ surface including 36 Co atoms and 18 C atoms, six Co layers and three C layers are contained in the model, this surface has three different adsorption sites: top site, bridge site and threefold hollow site. For the $Co_2C(011)$ surface including 36 Co atoms and 18 C atoms, four equivalent (010) Co layers and four C layers are contained in the model, four different adsorption sites exist: top site, bridge site, threefold hollow site and fourfold hollow site. During the calculations, the bottom two Co layers including C atoms are fixed; other layers and the adsorbates are fully relaxed.

All of the periodic DFT calculations are implemented using the Vienna Ab initio Simulation Package (VASP).[18−20] To compare the FTS selectivity over $Co_2C(101)$, (011), (010), (110), and (111) surfaces, all computational details over $Co_2C(010)$ and (011) surfaces are the same with our recent studies over $Co_2C(101)$, (110), and (111) surfaces,[3] which are presented in the part 1 of the Supporting Information.

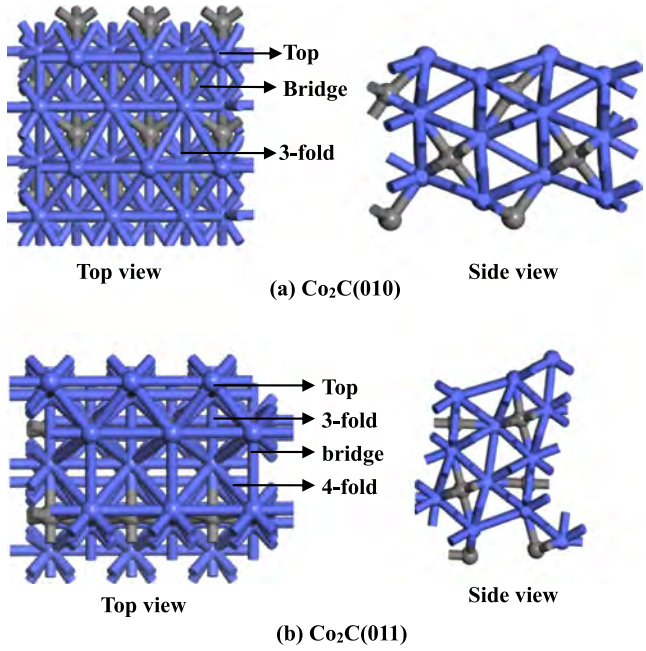

Figure 1. Surface morphology and the corresponding adsorption sites of (a) $Co_2C(010)$ and (b) $Co_2C(011)$.

3. RESULTS AND DISCUSSION

Because CO activation is usually believed to be the rate-limiting step in the FTS reactions and the key steps to form the monomer CH_x species,[21−23] the CO activation has been examined on the $Co_2C(110)$ and (111) surfaces that CO prefers hydrogen-assisted dissociation,[16] and CO activation was further examined on the exposed $Co_2C(101)$, (011), and (010) surfaces corresponding to the surface area proportions of 40.72, 35.21, and 11.80%, respectively. As illustrated in Figure S1, on the (101) surface, CO prefers hydrogen-assisted dissociation to form CH species with an activation free energy of 1.59 eV; on the (010) surface, CO prefers hydrogen-assisted dissociation to form CH species with an activation free energy of 2.40 eV; on the (011) surface, CO direct dissociation is the most favorable in kinetics than CO hydrogen-assisted dissociation (1.14 vs 1.62 eV). As a result, the Co_2C catalyst has enough active sites for CO non-dissociative adsorption, as well as CO direct and hydrogen-assisted dissociation to form the key CH_x (x = 1−3) intermediates.

On the basis of the above analysis, CH_x (x = 1−3), CO, and H species are considered to be the abundant and key intermediates to identify the selectivity of FTS reaction, which can contribute to the formation of C_2 species (C_2H_xO and C_2H_x) by CO insertion into CH_x (x = 1−3) and CH_x + CH_y (x, y = 1−3) coupling; meanwhile, the conversion of CH_x (x = 1−3) and its hydrogenation to CH_4 are considered. Table 1 lists the corresponding energy values of all elementary reactions related to CH_x (x = 1−3) species over $Co_2C(010)$ and (011) at 493 K. The only one imaginary frequency corresponding to the transition state involving in the reactions is listed in Table S1. The adsorption free energy, the key structural parameters, and the most stable configurations of all adsorbed species over $Co_2C(010)$ and (011) surfaces are presented in the part 4 of the Supporting Information.

To further investigate the catalytic activity of the involved reaction and the selectivity of C_2 species, the effective barrier and the effective barrier difference are employed to

DOI: 10.1021/acs.jpcc.8b08783
J. Phys. Chem. C 2018, 122, 29249−29258

Table 1. Elementary Reactions and the Corresponding Activation Free Energy (ΔG_a/eV), Reaction Free Energies (ΔG/eV) and the Effective Barrier (E_{eff}/eV) at 493 K for CH_x (x = 1−3) Species on the Co_2C(010) and (011) Surfaces[a]

		Co_2C(010)			Co_2C(011)		
reactions	transition states	ΔG_a	ΔG	E_{eff}	ΔG_a	ΔG	E_{eff}
CH + H═CH_2	TSn-1	0.90	0.69	0.91	0.72	0.28	0.84
CH + CH═C_2H_2	TSn-2	1.24	0.77	1.26	1.45	0.28	1.80
CH + CH_2═$CHCH_2$	TSn-3	0.58	−0.01	0.95	0.67	0.43	1.16
CH + CH_3═$CHCH_3$	TSn-4	1.47	0.33	2.01	0.99	0.13	1.52
CH_2═CH + H	TSn-6	0.21	−0.69	0.52	0.44	−0.28	0.70
CH_2 + H═CH_3	TSn-7	0.47	0.20	0.84	0.34	−0.36	0.70
CH_2 + CH_2═C_2H_4	TSn-8	1.19	0.71	1.91	0.55	−0.68	1.19
CH_2 + CH_3═CH_2CH_3	TSn-9	1.51	0.21	2.34	1.73	−0.14	2.41
CH_3═CH_2 + H	TSn-11	0.27	−0.20	0.76	0.70	0.36	1.07
CH_3 + H═CH_4	TSn-12	1.11	0.27	1.70	0.56	−0.12	0.94
CH_3 + CH_3═C_2H_6	TSn-13	2.00	−0.15	3.13	1.88	−0.24	2.63
CH + CO═CHCO	TSn-5	1.13	0.65	1.17	1.12	0.78	1.24
CH_2 + CO═CH_2CO	TSn-10	1.10	0.84	1.49	0.87	0.82	1.18
CH_3 + CO═CH_3CO	TSn-14	1.81	0.20	2.25	0.46	−0.21	0.75

[a] n = 1, 2 and 3 represent the transition states on the Co_2C(010) and (011) surfaces, respectively.

quantitatively evaluate the catalytic activity and selectivity, respectively; first, the coverage of CH_x (x = 1−3) species, θ_{CH_i}, can be expressed with respect to C coverage (θ_C) on Co_2C surface by the eq 1.[24,25]

$$\theta_{CH_i} = e^{-E_i/RT}\theta_C(\theta_H/\theta_*)^i = e^{-E_i/RT}\theta_C t^i \quad (1)$$

where t is θ_H/θ_* and E_i is the energy difference between the adsorbed CH_i and C + iH.

The CH_x formation and dissociation rate (rCH_i^{form} and rCH_i^{dis}) can be obtained according to the eqs 2 and 3[25−28]

$$r_{CH_i}^{form} = Ae^{-E_a^{hy}/RT}\theta_{CH_{i-1}}\theta_H = Ae^{-E_a^{hy}+E_{i-1}/RT}t^{i-1}\theta_C\theta_H = Ae^{-E_{eff,CH_i}/RT}t^{i-1}\theta_C\theta_H \quad (2)$$

$$r_{CH_i}^{dis} = Ae^{-E_a^{dis}/RT}\theta_{CH_i}\theta_* = Ae^{-E_a^{dis}+E_i/RT}t^i\theta_C\theta_* = Ae^{-E_{eff,CH_i}/RT}t^i\theta_C\theta_* \quad (3)$$

where A is the pre-exponential factor, E_a^{hy} is the barrier of CH_{i-1} hydrogenation, and E_a^{dis} is the barrier of CH_i dissociation. E_i and E_{i-1} are the relative stability of CH_i and CH_{i-1}, respectively, with respect to C atom. The effective barrier of CH_i formation (E_{eff}, CH_i^{form}) is equal to E_a^{hy} + E_{i-1}, and the effective barrier of CH_i dissociation (E_{eff}, CH_i^{dis}) is equal to E_a^{dis} + E_i.

The formation rates of C_2 hydrocarbons and oxygenates are calculated by the eqs 4 and 5[25−28]

$$r_{CH_i+CH_j} = Ae^{-E_a^{i,j}/RT}\theta_{CH_i}\theta_{CH_j} = Ae^{(-E_a^{i,j}+E_i+E_j)/RT}t^{i+j}\theta_C{}^2 = Ae^{-E_{eff,CH_i+CH_j}/RT}t^{i+j}\theta_C{}^2 \quad (4)$$

$$r_{CH_i+CO} = Ae^{-E_a^{i,CO}/RT}\theta_{CH_i}\theta_{CO} = Ae^{(-E_a^{i,CO}+E_i)/RT}t^i\theta_C\theta_{CO} = Ae^{-E_{eff,CH_i+CO}/RT}t^i\theta_C\theta_{CO} \quad (5)$$

where $r_{CH_i+CH_j}$ and r_{CH_i+CO} represent the reaction rate of CH_i + CH_j coupling and CO insertion into CH_i, respectively. $E_{i,j}^a$ and $E_{i,CO}^a$ are the barriers for the reactions of CH_i + CH_j coupling and CO insertion into CH_i, respectively. E_i and E_j are the relative stability of CH_i and CH_j with respect to C atom, respectively. $E_{eff,CH_i+CH_j} = E_{i,j}^a + E_i + E_j$ and $E_{eff,CH_i+CO} = E_{i,CO}^a + E_i$ are the effective barriers for the reactions of CH_i + CH_j coupling and CO insertion into CH_i, respectively. As mentioned above, the smaller the value of E_{eff} is, the higher the catalytic activity is.

The total C_2 species formation rate is expressed by the following equations

$$r_{C_2H_x} = \sum_{i=1}^{3}\sum_{j=1}^{3} r_{CH_i+CH_j} \approx \max(r_{CH_i+CH_j}) \quad (6)$$

$$r_{C_2H_yO} = \sum_{i=1}^{3} r_{CH_i+CO} \approx \max(r_{CH_i+CO}) \quad (7)$$

$$E_{eff,C_2H_x} = \min(E_{eff,CH_i+CH_j}) \quad (8)$$

$$E_{eff,C_2H_yO} = \min(E_{eff,CH_i+CO}) \quad (9)$$

According to the eqs 6 and 7, the ratio of C_2H_x formation rate to C_2H_xO formation rate can be expressed by the eq 10

$$\frac{r_{C_2H_x}}{r_{C_2H_yO}} = e^{-\Delta E_{eff}/RT} \times X \qquad X = t^{(i+j)-i}\theta_C/\theta_{CO} \quad (10)$$

where $\Delta E_{eff} = E_{eff,C_2H_x} - E_{eff,C_2H_xO}$ is the effective barrier difference between C_2H_x and C_2H_xO formation. It is worth mentioning that $\frac{r_{C_2H_x}}{r_{C_2H_yO}}$ depends on ΔE_{eff} exponentially,[27−29] for example, the value of ΔE_{eff} changes by 0.1 eV, $\frac{r_{C_2H_x}}{r_{C_2H_yO}}$ will change 10-fold at 493 K. Thus, the effect of ΔE_{eff} is more obvious than θ_C/θ_{CO} and t, namely, the relative concentration of CO/CH_x little affects the analysis toward selectivity, and as a result, the value of ΔE_{eff} can be used as a good descriptor to qualitatively measure the selectivity of C_2 species. Moreover, the smaller the value of ΔE_{eff} is, the higher the selectivity of C_2H_x formation is, whereas the larger the value of ΔE_{eff}, the higher the selectivity of C_2H_xO formation is.

3.1. Formations of C_2 Species on the Co_2C(010) Surface. To investigate the formation of C_2 species, the reactions related to key intermediates CH_x (x = 1−3), CO, and

DOI: 10.1021/acs.jpcc.8b08783
J. Phys. Chem. C 2018, 122, 29249−29258

H are examined. Figure 2 presents the potential energy for CO insertion into CH_x (x = 1−3) and CH_x + CH_y (x, y = 1−3)

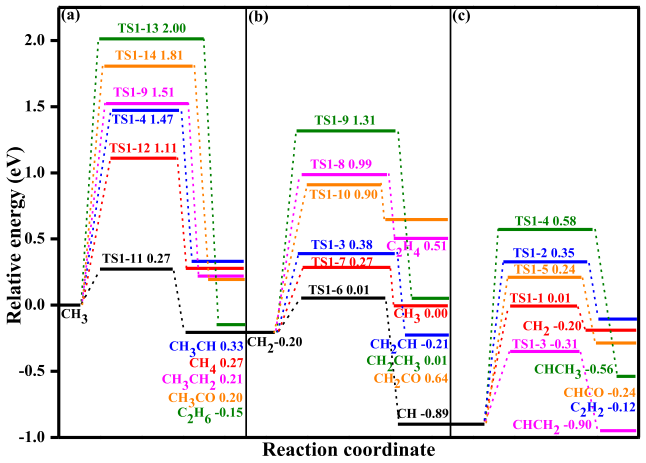

Figure 2. Potential energy profile of Gibbs free energy (493 K) for the reactions related to (a) CH_3, (b) CH_2, and (c) CH species on the $Co_2C(010)$ surface together with the corresponding structures in Figure 3.

coupling, as well as the conversion of CH_x (x = 1−3) and its hydrogenation to CH_4 on $Co_2C(010)$ surface at 493 K (Figure 3).

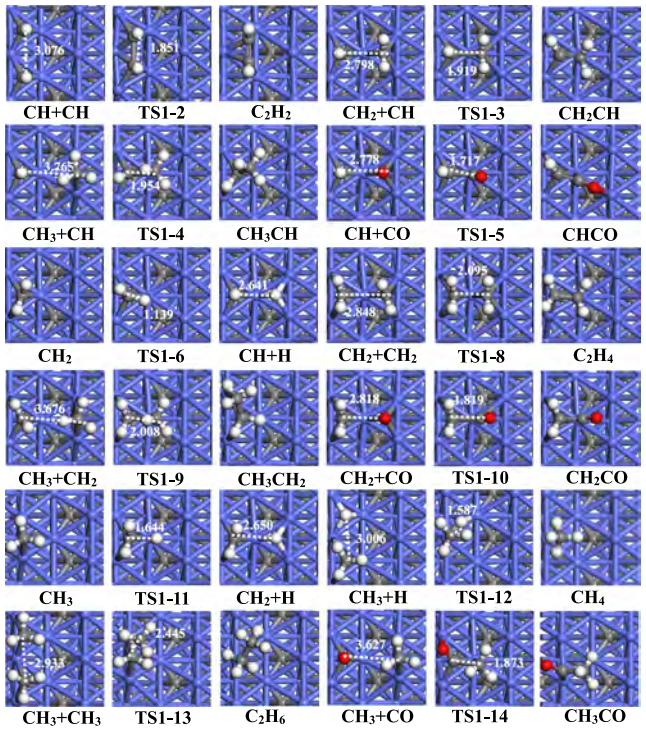

Figure 3. Structures of initial states (ISs), transition states (TSs), and final states (FSs) of the all reactions related to CH_x (x = 1−3) species on the $Co_2C(010)$ surface. CH hydrogenation to CH_2 and CH_2 hydrogenation to CH_3 are the reverse reactions of CH_2 dissociation into CH and CH_3 dissociation into CH_2, respectively; only the structures of CH_2 dissociation into CH and CH_3 dissociation into CH_2 are presented. Co, C, H, and O atoms are shown in the blue, gray, white, and red balls, respectively. Bond length is in Å.

As illustrated in Figure 2a, for the CH_3 species, CH_3 dissociation into CH_2 is the most favorable with the lowest activation free energy of 0.27 eV, and it is exothermic by 0.20 eV. The second is CH_3 hydrogenation to CH_4 with the activation free energy of 1.11 eV, whereas it is endothermic by 0.27 eV. Meanwhile, the difference of activation free energy between these two reactions is 0.84 eV, suggesting that CH_3 species would completely dissociate into CH_2 species instead of its hydrogenation to CH_4. The third is CH_3 coupling with CH to CH_3CH with the activation and reaction free energies of 1.47 and 0.33 eV. The last three reactions are CH_3 coupling with CH_2, CO insertion into CH_3, and CH_3 coupling with CH_3, which have the high activation free energies of 1.51, 1.81, and 2.00 eV, and the corresponding reaction free energies of 0.21, 0.20, and −0.15 eV, respectively. As a result, the latter four reactions are difficult to occur for CH_3 species. On the other hand, the effective barrier (see Table 1) is used to quantitatively evaluate the activity, which includes the coverage of CH_x, CO, and H species, as well as the available sites, θ_{CH_x}, θ_{CO}, θ_H, and θ_*, and the results show that the most favorable reaction is still CH_3 dissociation into CH_2 with the smallest effective barrier of 0.76 eV; the second is CH_3 hydrogenation to CH_4 with the activation free energy of 1.70 eV. Thus, CH_3 dissociation into CH_2 is the most favorable both kinetically and thermodynamically among all reactions related to CH_3 species.

For the CH_2 species, as presented in Figure 2b, CH_2 dissociation into CH has the lowest activation free energy of 0.21 eV. The second is CH_2 hydrogenation to CH_3 with the activation free energy of 0.47 eV. The third is CH_2 coupling with CH with the activation free energy of 0.58 eV. These three reactions correspond to the effective barrier of 0.52, 0.84, and 0.95 eV. Thus, CH_2 dissociation into CH is more favorable in kinetics.

For the CH species, as shown in Figure 2c, CH coupling with CH_2 to $CHCH_2$ is the most favorable; the second is CH hydrogenation to CH_2; both reactions have the activation free energies of 0.58 and 0.90 eV, respectively. However, as listed in Table 1, the effective barrier of CH hydrogenation to CH_2 (0.91 eV) is close to that of CH coupling with CH_2 to $CHCH_2$ (0.95 eV). Hence, CH coupling with CH_2 to $CHCH_2$ and CH hydrogenation to CH_2 are two parallel reactions.

3.2. Formation of C_2 Species on $Co_2C(011)$ Surface. As illustrated in Figure 4a, for all reactions related to CH_3 species, CO insertion into CH_3 has the lowest activation free energy of 0.46 eV, the second is CH_3 hydrogenation to CH_4 with the activation free energy of 0.56 eV, and the third is CH_3 dissociation into CH_2 with the activation free energy of 0.70 eV. Meanwhile, the corresponding effective barriers are 0.75, 0.94, and 1.07 eV, respectively. Thus, CO insertion into CH_3 is the most favorable.

For all reactions related to CH_2 species, as presented in Figure 4b, the former three favorable reactions are CH_2 hydrogenation to CH_3, CH_2 dissociation into CH, and CH_2 self-coupling to C_2H_4, which have the activation free energies of 0.34, 0.44, and 0.55 eV, respectively; the corresponding effective barriers are 0.70, 0.70, 1.19 eV, respectively. Thus, CH_2 hydrogenation to CH_3 and CH_2 dissociation into CH are two parallel and favorable reactions in kinetics (Figure 5).

For all reactions related to CH species, as shown in Figure 4c, the first three favorable reactions are CH + CH_2 coupling to CH_2CH, CH hydrogenation to CH_2, and CH + CH_3 coupling to CH_3CH with the activation free energies of 0.67,

DOI: 10.1021/acs.jpcc.8b08783
J. Phys. Chem. C 2018, 122, 29249−29258

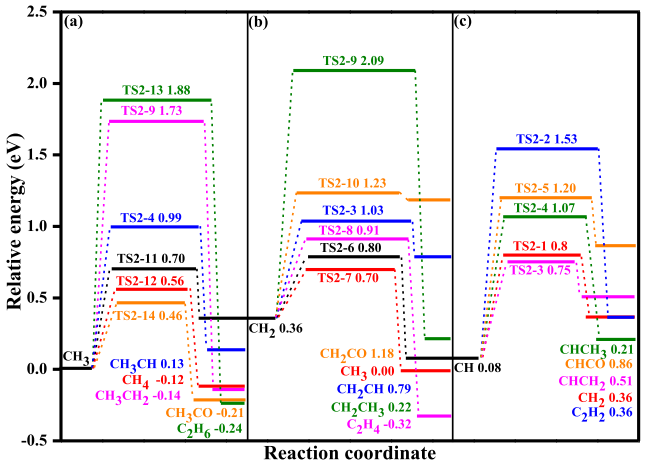

Figure 4. Potential energy profile of Gibbs free energy (493 K) for the reactions related to (a) CH_3, (b) CH_2, and (c) CH species on the $Co_2C(011)$ surface together with the corresponding structures in Figure 5.

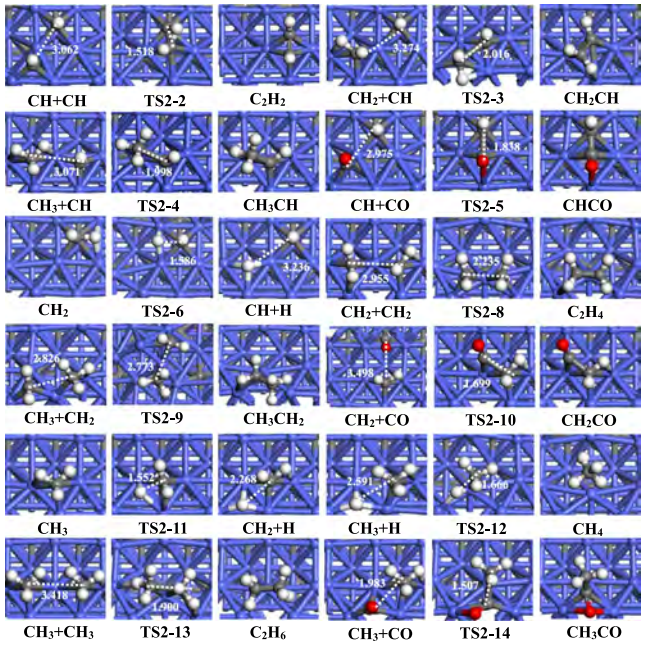

Figure 5. Structures of ISs, TSs, and FSs of the all reactions related to CH_x (x = 1−3) species on the $Co_2C(011)$ surface. CH hydrogenation to CH_2 and CH_2 hydrogenation to CH_3 are the reverse reactions of CH_2 dissociation into CH and CH_3 dissociation into CH_2, respectively; only the structures of CH_2 dissociation into CH and CH_3 dissociation into CH_2 are presented. Co, C, H, and O atoms are shown in the blue, gray, white and red balls, respectively. Bond length is in Å.

0.72, and 0.99 eV, which have the corresponding effective barriers of 1.16, 0.84, and 1.52 eV, respectively. As a result, CH prefers to be hydrogenated to CH_2 in kinetics.

3.3. General Discussions. *3.3.1. Effect of Co_2C Crystal Facets on the Existence Form of CH_x and Product Distribution.* As mentioned above, for the (010) surface, starting from CH_3 species, it prefers to be dissociated into CH_2, followed by its dissociation into CH; however, for the CH species, its hydrogenation to CH_2 and its coupling with CH_2 to CH_2CH are two parallel reactions, suggesting that the conversion between CH and CH_2 species easily occur, both CH and CH_2 species are the dominant CH_x monomer. Further, CH coupling with CH_2 to CH_2CH is the dominant reaction to form C_2 species. Thus, the $Co_2C(010)$ surface exhibits a high catalytic activity and selectivity toward the formation of C_2 hydrocarbons CH_2CH rather than C_2 oxygenates.

For the (011) surface, although CH_2 hydrogenation and its dissociation are two parallel favorable reactions, CH prefers to be hydrogenated to CH_2, suggesting that once CH and CH_2 species are formed, both prefer to be hydrogenated to CH_3, which is the dominant CH_x monomer. Starting from CH_3 species, CO insertion into CH_3 to CH_3CO is the dominant reaction to form C_2 species. Thus, different from the $Co_2C(010)$ surface, the $Co_2C(011)$ surface exhibits a high catalytic activity and selectivity toward the formation of C_2 oxygenates CH_3CO instead of C_2 hydrocarbons.

Taking our previous studies[3] over $Co_2C(101)$, (110), and (111) surfaces into consideration, Table 2 summarizes the dominant existence form of CH_x monomer and the dominant C_2 species over five exposed Co_2C surfaces. On the (111) surface, CH is the dominant CH_x monomer, CO insertion into CH contributes to the formation of C_2 oxygenate (CHCO); on the (101) surface, CH is the dominant CH_x monomer; on the (110) surface, both CH and CH_2 are the dominant CH_x monomer; accordingly, on the (101) and (110) surfaces, CH self-coupling and CH coupling with CH_2 lead to the formation of C_2 hydrocarbons (C_2H_2 and CH_2CH), respectively.

Above results show that the crystal facets of Co_2C catalyst affect the dominant existence form of CH_x species and therefore alter the favorable pathway of the reactions related to CH_x species to form C_2 species, which ultimately leads to different selectivity of the product; namely, the product distribution of C_2 species and the dominant existence form of CH_x species over Co_2C catalyst in FTS reaction is sensitive to its crystal facet.

3.3.2. Selectivity between C_2 Oxygenates and C_2 Hydrocarbons. Figure 6 demonstrates the effective barrier profile for the most favorable formation pathways of C_2 oxygenates and hydrocarbons on $Co_2C(011)$, (111), (010), (110), and (101) surfaces.

On the (011), CO insertion into CH_3 to CH_3CO is much more favorable in kinetics than CH_3 coupling with CH to CH_3CH (0.75 vs 1.52 eV). On the (111), CO insertion into CH to CHCO is more facile than CH self-coupling to C_2H_2 (1.08 vs 1.41 eV). However, on the $Co_2C(010)$ and (110), CH coupling with CH_2 to CH_2CH (0.95 and 0.56 eV) is easier than C_2 oxygenates formation by CO insertion into CH (1.17 and 1.38 eV), which are also more favorable than CO insertion into CH_2 (1.49 and 1.65 eV), respectively. On the $Co_2C(101)$, CH self-coupling to C_2H_2 is more facile than CO insertion into CH to CHCO (0.93 vs 1.20 eV).

On the other hand, the selectivity between C_2 hydrocarbons C_2H_x (CH_2CH and C_2H_2) and C_2 oxygenates C_2H_xO (CHCO and CH_3CO) over the (011), (111), (010), (110), and (101) surfaces is quantitatively described by the effective barrier difference between C_2H_x and C_2H_xO (see Table 2), and the ΔE_{eff} values of 0.77 and 0.33 eV over the (011) and (111) surfaces mean that these two surfaces have a higher selectivity toward the formation of C_2 oxygenates (C_2H_xO). However, the ΔE_{eff} are −0.22, −0.27, and −0.82 eV over the (010), (101), and (110) surfaces, suggesting that these three surfaces have good selectivity toward the formation of C_2 hydrocarbons (C_2H_x). Thus, for the Co_2C catalyst, both (011) and (111)

DOI: 10.1021/acs.jpcc.8b08783
J. Phys. Chem. C 2018, 122, 29249−29258

Table 2. Effective Barrier for the Formation Reaction of C_2H_x and C_2H_xO Species on the Co_2C(011), (111), (010), (101) and (110) Surfaces[a]

surfaces	CH_x monomer	C_2 species		E_{eff,C_2H_x}/eV	E_{eff,C_2H_xO}/eV	ΔE_{eff}/eV
(011)	CH_3	CH_3CH	CH_3CO	1.52	0.75	0.77
(111)	CH	C_2H_2	CHCO	1.41	1.08	0.33
(010)	CH, CH_2	CH_2CH	CHCO	0.95	1.17	−0.22
(101)	CH	C_2H_2	CHCO	0.93	1.20	−0.27
(110)	CH, CH_2	CH_2CH	CHCO	0.56	1.38	−0.82

[a]It is noted that the values of E_{eff,C_2H_x} denotes CH_3CH, CH_2CH and C_2H_2 formations on the Co_2C surfaces, E_{eff,C_2H_xO} denotes CHCO and CH_3CO formation on the Co_2C surfaces, respectively.

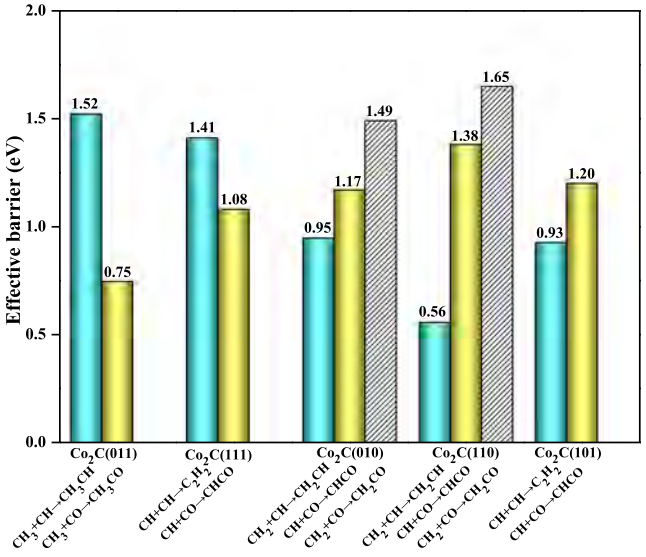

Figure 6. Effective barrier profile for the favorable formation pathways of C_2 oxygenates and hydrocarbons on the Co_2C(011), (111), (010), (110), and (101) surfaces.

crystal facets with the surface area proportion of 35.21 and 0.27% are dominantly responsible for the formation of C_2 oxygenates, whereas the (010), (101), and (110) crystal facets with the surface area proportion of 11.80, 40.72, and 9.87% mainly contribute to the formation of C_2 hydrocarbons. These results show that the selectivity of C_2 species between oxygenates and hydrocarbons over the Co_2C catalyst in the FTS reaction is also sensitive to its crystal facet, which give out a microscopic explanation about two different views for the role of Co_2C active phase as mentioned in Introduction: one is for the formation of lower olefin and the other is for the formation of higher alcohol.

Correspondingly, under the realistic FTS conditions, aiming at obtaining high selectivity of C_2 oxygenates, more (011) and (111) crystal facets should be exposed, whereas more (010), (101), and (110) crystal facets should be exposed for the formation of C_2 hydrocarbons. Moreover, previous experiments[1,10] have confirmed that the Co_2C nanoprisms with the dominantly exposed (101) crystal facet favors the production of lower olefins, which further support our calculated results.

It is noted that when CO insertion mechanism to form C_2 oxygenates (C_2H_xO) is more favorable than CH_x coupling to C_2 hydrocarbons (C_2H_x) over the Co_2C surfaces, the C−O bond scission of C_2H_xO to form C_2H_x may be favorable than its hydrogenation to higher alcohols, which may alter the product selectivity and needs to be further analyzed. Since both (011) and (111) crystal facets are in favor of C_2 oxygenates formation, both facets correspond to surface area proportion of 35.21 and 0.27%, respectively, as a result, the (011) facet occupying a large proportion of surface area should be dominantly responsible for most of C_2 oxygenates formation instead of the (111) facet. As a result, the C−O bond scission and hydrogenation of C_2H_xO over the Co_2C(011) are examined, as illustrated in Figure S5, and starting from the dominant C_2 oxygenates CH_3CO, its hydrogenation to CH_3CHO is more favorable in kinetics than CH_3COH formation (0.52 vs 1.52 eV); then, CH_3CHO hydrogenation to CH_3CHOH is much easier in kinetics than the C−O bond scission of CH_3CHO to CH_3CH (0.48 vs 1.11 eV); further, CH_3CHOH hydrogenation to ethanol has the activation free energy of 0.28 eV. Moreover, the FTS reactions usually occurred under the hydrogen-rich conditions, which promote CH_3CHO successive hydrogenation to ethanol rather than its C−O bond scission to CH_3CH. Therefore, the CO insertion chain growth mechanism is more favorable than CH_x coupling in kinetics over the Co_2C(011) crystal facet, C_2H_xO prefers to be hydrogenated to form ethanol instead of its C−O bond scission to C_2 hydrocarbons, and C_2 oxygenates as the precursor of ethanol could be used to evaluate the selectivity of higher alcohols from syngas under the hydrogen-rich conditions.

3.3.3. Selectivity between C_2 Species and CH_4. In the FTS reaction, expect for the dominant C_{2+} products, the formation of CH_4 also affects the selectivity of C_{2+} species.[1,30−32] DFT study by Cheng et al.[28] showed that CH_4 can be formed on the Co_2C catalyst. However, the experiments[1,10] have confirmed that Co_2C nanoprisms with the dominantly exposed (101) facet favor the production of lower olefins and inhibit CH_4 formation. It is therefore assumed that CH_4 formation may be also sensitive to the crystal facets of Co_2C catalyst. To illustrate the effect of Co_2C crystal facet on CH_4 formation, we compared the most favorable pathway related to CH_3 species with CH_4 formation by CH_3 hydrogenation on the five Co_2C surfaces. Figure 7 demonstrates the effective barrier of the most favorable pathway related to CH_3 species compared with CH_4 formation by CH_3 hydrogenation on the five Co_2C surfaces.

On the (011), CO insertion into CH_3 to CH_3CO is more favorable in kinetics than CH_4 formation by CH_3 hydrogenation (0.75 vs 0.94 eV). On the (111), (010), and (101), CH_3 hydrogenation to CH_4 is difficult compared with CH_3 dissociation into CH_2 (2.28 vs 2.00, 1.70 vs 0.76, 1.54 vs 1.08 eV); meanwhile, the formed CH_2 species can participle into the dissociation into CH, followed by its interaction with CO, its coupling with CH_2 or CH to form C_2 species; all these reactions are also easier than CH_3 hydrogenation to CH_4; namely, the formation of C_2 species is more favorable than

DOI: 10.1021/acs.jpcc.8b08783
J. Phys. Chem. C 2018, 122, 29249−29258

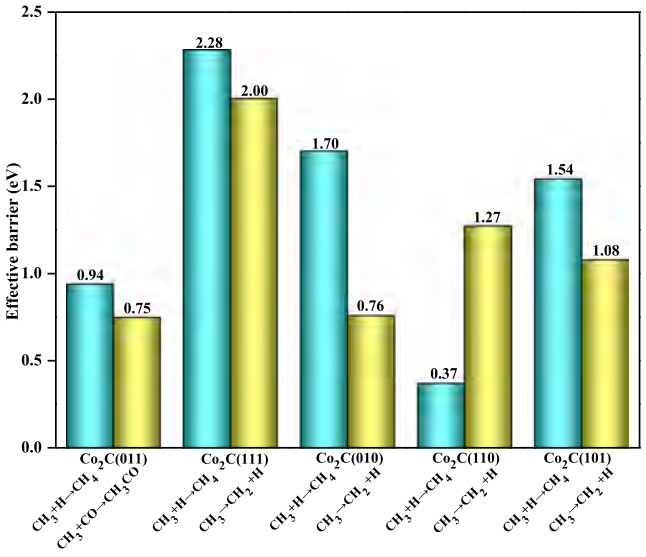

Figure 7. Effective barrier of the favorable pathways related to CH_3 and CH_3 hydrogenation to CH_4 on the $Co_2C(011)$, (111), (010), (110), and (101) surfaces.

CH_4 formation. However, on the (110), CH_3 hydrogenation to CH_4 is much more favorable in kinetics than CH_3 dissociation into CH_2 (0.37 vs 1.27 eV); the formed CH_2 species couples with its dissociation species CH to form C_2 species, which is not favorable compared with CH_4 formation by CH_3 hydrogenation, suggesting that CH_4 formation is more favorable than C_2 species. On the other hand, the effective barrier difference between the favored species and CH_4 over the (011), (111), (010), (110), and (101) surfaces are 0.19, 0.28, 0.94, −0.90, and 0.46 eV, respectively.

Above results show that only the (110) surface with the surface area proportion of 9.87% has higher selectivity toward CH_4 formation compared with C_2 species among five types of Co_2C surfaces. Other four types of (011), (111), (010), and (101) surfaces with the total surface area proportion of 88.05% have much higher selectivity toward C_2 species rather than CH_4, especially for the exposed (101) surface, the experiments[1,10] have confirmed that this surface can inhibit CH_4 formation. Overall, the Co_2C catalyst exhibits higher selectivity toward the formation of C_2 species.

3.3.4. Electronic and Structural Properties of Co_2C Crystal Facets. On the basis of the above DFT results, the Co_2C catalyst exhibits the sensitivity of crystal facets toward the product selectivity in the FTS reaction; aiming at providing a physical insight to illustrate the relationship between the sensitivity of C_2 species and Co_2C crystal facets, the electronic and structural properties of different Co_2C crystal facets are examined.

In the view of electronic properties, as shown in Figure 8, on the basis of the projected density of states (pDOS), the d-band energies of different Co_2C crystal facets are −1.52, −1.59, −1.63, −1.72, and −1.74 eV, which correspond to the (011), (111), (010), (110), and (101) facets, respectively. Previous studies about CO insertion into CH_x fragment to form the C−C bond[33] show that the doubly occupied 5σ CO orbital interacts with the occupied σ-CH_x orbital, namely, the doubly occupied bonding and anti-binding orbital would cause the repulsive interaction. Our results show that the upshift of the (011) and (111) surface d-band center can empty more antibonding states to reduce the repulsion, as a result, CO

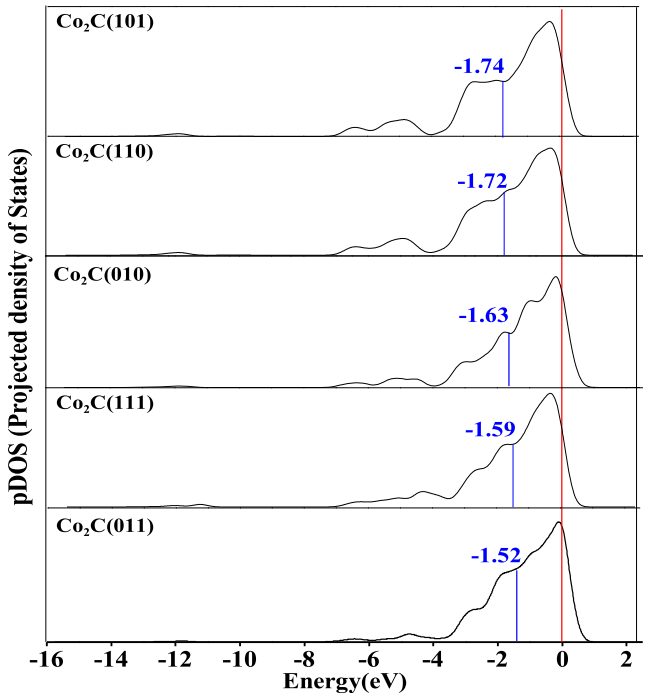

Figure 8. pDOS for surface Co atoms over the Co_2C catalyst. The blue solid line indicates the d-band center; the red solid line denotes Fermi level.

insertion into CH_x is easier to occur on the (011) and (111) facets, as shown below, both the (011) and (111) facets expose much denser B_5-type active unit. On the contrary, the downshift of the (010), (101), and (110) surfaces d-band center empty less antibonding states to restrain CO insertion into CH_x. The analyses of electronic properties are in agreement with our kinetics results.

In the view of structural properties, Figure 9 exhibits the surface morphology of $Co_2C(011)$, (111), (010), (101), and

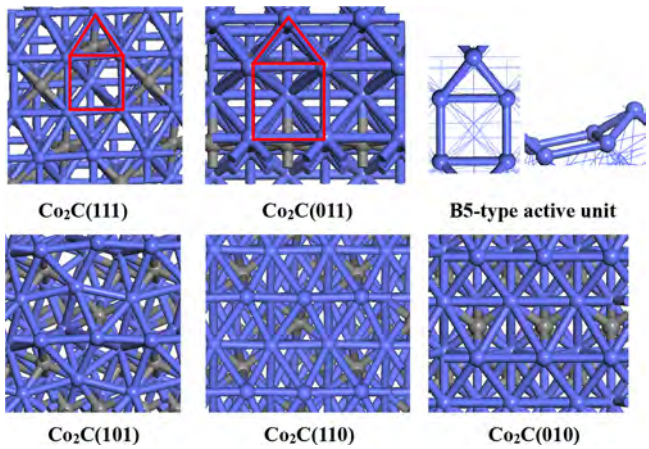

Figure 9. Surface morphology of $Co_2C(111)$, (011), (101), (110), and (010) surfaces together with the corresponding structure of B5-type active unit.

(110) surfaces, as well as the structure of B_5-type active unit. It is found that both (011) and (111) surfaces have four adsorption sites: top, bridge, threefold and fourfold hollow sites. The (010), (101), and (110) surfaces have three adsorption sites: top, bridge, and threefold hollow sites. As a

DOI: 10.1021/acs.jpcc.8b08783
J. Phys. Chem. C 2018, 122, 29249−29258

result, both threefold and fourfold hollow sites over the (011) and (111) surfaces constitute the special B_5-type active unit with five Co atoms, and then, the B_5-type active units consist of much denser active sites; further, Co_2C crystal facet with the B_5-type active unit have high selectivity toward C_2 oxygenates. However, Co_2C crystal facets without the special B_5-type active unit exhibit high selectivity toward CH_4 and C_2 hydrocarbons.

As mentioned above, Co_2C with the B_5-type active site can facilitate the formation of CH_x intermediates by CO direct dissociation to C, followed by its successive hydrogenations; meanwhile, it can promote CO insertion into CH_x to form C_2 oxygenates on the basis of its specific electronic properties to reduce the repulsion between CO and CH_x. In addition, the B_5-type active site also plays an important role in the CO activation. For example, Liu et al.[34] confirmed that HCP Co is more active than the FCC Co; meanwhile, HCP Co prefers CO direct dissociation and FCC Co prefers CO H-assisted dissociation, and the B_5-type sites can promote CO activation. CO activation on Ru catalysts[21,35] is similar to Co catalysts, in which Ru catalysts with B_5-type active site prefer CO direct dissociation to facilitate CO activation based on experiment and DFT study.

On the other hand, CO activation could be used as a descriptor to evaluate the activity of FTS catalyst over Co[34] and Ru[35] catalysts. Meanwhile, Figure 10 shows the pathways

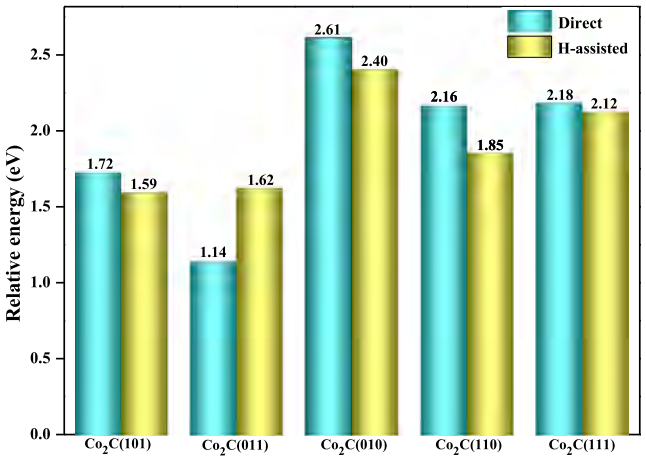

Figure 10. Highest activation free energy of CO activation via the direct and H-assisted dissociation to form CH species on the Co_2C(101), (011), (010), (110), and (111) surfaces.

of CO activation to form CH on the Co_2C(101), (011), (010), (110),[16] and (111)[16] surfaces. These results shown that CO prefers the nondissociative adsorption and hydrogen-assisted dissociation on the Co_2C(101), (010) and (110) surfaces, whereas CO prefers direct dissociation on the (011) surface; CO direct and hydrogen-assisted dissociation are two parallel reactions on the Co_2C(111) surface. CO direct and hydrogen-assisted dissociation on the Co_2C surfaces are compared with those on the HCP Co(10−11) and FCC Co(311) surfaces[15,34] with high catalytic activity for CO dissociation. These results suggested that Co_2C(011) surface with the B_5-type active unit has higher activity for CO dissociation than Co(10−11) and (311) facets (1.14 vs 1.21 and 1.36 eV), whereas CO dissociation on the Co_2C(101), (010), (110), and (111) surfaces are more difficult than Co(10−11) and (311) surfaces (1.59, 2.40, 1.85, 2.12 vs 1.21, 1.36 eV). Therefore, the Co_2C(011) crystal facet with the B_5-type active unit can present high activity for CO dissociation than Co catalysts, whereas the Co_2C(111) facet with the B_5-type active unit and Co_2C crystal facets without the B_5-type active unit exhibit low activity than Co catalysts. In addition, it is noted that although both Co_2C(011) and (111) facets have the B_5-type active unit, the Co_2C(011) facet only exposed Co atoms, whereas Co_2C(111) facet exposed the surface Co and C atoms; the surface C atoms adsorbed at fourfold hollow site occupied the active sites of CO activation, which greatly reduced the number of active sites and went against CO activation.

Further, for the formation of C_2 oxygenates CH_3CO by CO insertion into CH_3 over the Co_2C(011) surface, it is noted that Co_2C(011) surface is highly active for CO dissociation with the activation barrier of 1.14 eV; however, CO insertion into CH_3 is still more favorable than CO direct dissociation in kinetics (0.46 vs 1.14 eV). Thus, it is concluded that a part of CO participates into the direct dissociation into C, followed by its successive hydrogenation to CH_3; meanwhile, a part of CO can participate into insertion reaction to form C_2 oxygenate CH_3CO. As a result, CO can exist in the form of nondissociative adsorption and hydrogen-assisted dissociation over the Co_2C(011) surface, which can exhibit high activity and selectivity toward the formation of C_2 oxygenates and ethanol.

4. CONCLUSIONS

Aiming at identifying the effects of Co_2C crystal facet on the selectivity of C_2 oxygenates and hydrocarbons in the FTS, the formation mechanism of C_2 species over five exposed Co-termination (101), (011), (010), (110), and (111) surfaces under the hydrogen-rich conditions in FTS reaction are examined using DFT calculations. The results show that the C−C bond of C_2 species prefers to be formed instead of C_1 species CH_4 over the dominantly exposed Co_2C crystal facets, and the selectivity of C_2 species and the dominant existence form of CH_x species are sensitive to the crystal facet of the Co_2C catalyst. On the (010) and (110), CH and CH_2 species are the dominant form of CH_x species, and CH_2 coupling with CH to CH_2CH is the dominant product. On the (011), CH_3 monomer is the dominant CH_x species, and CO insertion into CH_3 contributes to CH_3CO. On the (111), CO insertion into the dominant monomer CH can form CHCO. On the (101), the dominant monomer CH self-coupling to C_2H_2 is the dominant product.

The electronic and structural properties of different Co_2C crystal facets well illustrate the structure−selectivity relationship between FTS selectivity and Co_2C crystal facets, namely, the high selectivity of C_2 oxygenates over (011) and (111) surfaces are attributed to the presence of the step B_5-type active unit with five Co atoms, and these active units consist of much denser active sites; meanwhile, the d-band center of (011) and (111) surfaces is closer to the Fermi energy level, whereas there is high selectivity of C_2 hydrocarbons on the (101) and (010), as well as CH_4 on the (110). Therefore, the selectivity of C_2 species over Co_2C catalyst is closely associated with Co_2C crystal facet's electronic and structural properties; regulating the exposed crystal facet of Co_2C catalyst can control the selectivity of desirable C_2 species. This work provides a newly physical insight into the design of Co_2C catalysts to improve the selectivity of desired products in FTS reaction.

DOI: 10.1021/acs.jpcc.8b08783
J. Phys. Chem. C 2018, 122, 29249−29258

■ ASSOCIATED CONTENT

Supporting Information

The Supporting Information is available free of charge on the ACS Publications website at DOI: 10.1021/acs.jpcc.8b08783.

Computational details, methods for calculating the Gibbs free energy, CO activation on the Co_2C, the only one imaginary frequency corresponding to the transition state, most stable adsorption configurations of all adsorbed species, and the reactions related to the C−O bond scission or hydrogenation of C_2H_xO on the $Co_2C(011)$ surface (PDF)

■ AUTHOR INFORMATION

Corresponding Author

*E-mail: zhangriguang@tyut.edu.cn.

ORCID

Baojun Wang: 0000-0002-9069-6720

Notes

The authors declare no competing financial interest.

■ ACKNOWLEDGMENTS

This work is financially supported by the Key projects of National Natural Science Foundation of China (no. 21736007), the National Natural Science Foundation of China (nos. 21476155, 21776193), the China Scholarship Council (201606935026), the Top Young Innovative Talents of Shanxi, and U.S. NSF-sponsored NCAR-Wyoming Supercomputing Center (NWSC).

■ REFERENCES

(1) Zhong, L.; Yu, F.; An, Y.; Zhao, Y.; Sun, Y.; Li, Z.; Lin, T.; Lin, Y.; Qi, X.; Dai, Y.; et al. Cobalt Carbide Nanoprisms for Direct Production of Lower Olefins from Syngas. *Nature* **2016**, *538*, 84−87.

(2) Zhao, Z.; Lu, W.; Yang, R.; Zhu, H.; Dong, W.; Sun, F.; Jiang, Z.; Lyu, Y.; Liu, T.; Du, H.; et al. Insight into the Formation of Co@Co_2C Catalysts for Direct Synthesis of Higher Alcohols and Olefins from Syngas. *ACS Catal.* **2017**, *8*, 228−241.

(3) Zhang, R.; Wen, G.; Adidharma, H.; Russell, A. G.; Wang, B.; Radosz, M.; Fan, M. C_2 Oxygenate Synthesis via Fischer−Tropsch Synthesis on Co_2C and Co/Co_2C Interface Catalysts: How to Control the Catalyst Crystal Facet for Optimal Selectivity. *ACS Catal.* **2017**, *7*, 8285−8295.

(4) Fang, K.; Li, D.; Lin, M.; Xiang, M.; Wei, W.; Sun, Y. A Short Review of Heterogeneous Catalytic Process for Mixed Alcohols Synthesis via Syngas. *Catal. Today* **2009**, *147*, 133−138.

(5) Xiang, Y.; Kruse, N. Tuning the Catalytic CO Hydrogenation to Straight- and Long-Chain Aldehydes/Alcohols and Olefins/Paraffins. *Nat. Commun.* **2016**, *7*, 13058.

(6) Jiao, G.; Ding, Y.; Zhu, H.; Li, X.; Li, J.; Lin, R.; Dong, W.; Gong, L.; Pei, Y.; Lu, Y. Effect of La_2O_3 Doping on Syntheses of C_1−C_{18} Mixed Linear α-Alcohols from Syngas over the Co/AC Catalysts. *Appl. Catal., A* **2009**, *364*, 137−142.

(7) Fang, Y.; Liu, Y.; Deng, W.; Liu, J. Cu-Co Bi-metal Catalyst Prepared by Perovskite CuO/$LaCoO_3$ Used for Higher Alcohol Synthesis from Syngas. *J. Energy Chem.* **2014**, *23*, 527−534.

(8) Fang, Y. Z.; Liu, Y.; Zhang, L. H. $LaFeO_3$-Supported Nano Co-Cu Catalysts for Higher Alcohol Synthesis from Syngas. *Appl. Catal., A* **2011**, *397*, 183−191.

(9) Lebarbier, V. M.; Mei, D.; Kim, D. H.; Andersen, A.; Male, J. L.; Holladay, J. E.; Rousseau, R.; Wang, Y. Effects of La_2O_3 on the Mixed Higher Alcohols Synthesis from Syngas over Co Catalysts: A Combined Theoretical and Experimental Study. *J. Phys. Chem. C* **2011**, *115*, 17440−17451.

(10) Li, Z.; Zhong, L.; Yu, F.; An, Y.; Dai, Y.; Yang, Y.; Lin, T.; Li, S.; Wang, H.; Gao, P.; et al. Effects of Sodium on the Catalytic Performance of CoMn Catalysts for Fischer-Tropsch to Olefin Reactions. *ACS Catal.* **2017**, *7*, 3622−3631.

(11) Volkova, G. G.; Yurieva, T. M.; Plyasova, L. M.; Naumova, M. I.; Zaikovskii, V. I. Role of the Cu-Co Alloy and Cobalt Carbide in Higher Alcohol Synthesis. *J. Mol. Catal. A: Chem.* **2000**, *158*, 389−393.

(12) Pei, Y.; Ding, Y.; Zhu, H.; Zang, J.; Song, X.; Dong, W.; Wang, T.; Yan, L.; Lu, Y. Study on the Effect of Alkali Promoters on the Formation of Cobalt Carbide (Co_2C) and on the Performance of Co_2C via CO Hydrogenation Reaction. *React. Kinet. Mech. Catal.* **2013**, *111*, 505−520.

(13) Pei, Y.; Ding, Y.; Zang, J.; Song, X.; Dong, W.; Zhu, H.; Wang, T.; Chen, W. Fischer-Tropsch Synthesis: Characterizing and Reaction Testing of Co_2C/SiO_2 and Co_2C/Al_2O_3 Catalysts. *Chin. J. Catal.* **2015**, *36*, 252−259.

(14) Du, H.; Zhu, H.; Chen, X.; Dong, W.; Lu, W.; Luo, W.; Jiang, M.; Liu, T.; Ding, Y. Study on CaO-promoted Co/AC Catalysts for Synthesis of Higher Alcohols from Syngas. *Fuel* **2016**, *182*, 42−49.

(15) Dong, W.; Liu, J.; Zhu, H.; Ding, Y.; Pei, Y.; Liu, J.; Du, H.; Jiang, M.; Liu, T.; Su, H.; et al. Co-Co_2C and Co-Co_2C/AC Catalysts for Hydroformylation of 1-Hexene under Low Pressure: Experimental and Theoretical Studies. *J. Phys. Chem. C* **2014**, *118*, 19114−19122.

(16) Pei, Y.-P.; Liu, J.-X.; Zhao, Y.-H.; Ding, Y.-J.; Liu, T.; Dong, W.-D.; Zhu, H.-J.; Su, H.-Y.; Yan, L.; Li, J.-L.; et al. High Alcohols Synthesis via Fischer-Tropsch Reaction at Cobalt Metal/Carbide Interface. *ACS Catal.* **2015**, *5*, 3620−3624.

(17) Zhao, Y.-H.; Su, H.-Y.; Sun, K.; Liu, J.; Li, W.-X. Structural and Electronic Properties of Cobalt Carbide Co_2C and Its Surface Stability: Density Functional Theory Study. *Surf. Sci.* **2012**, *606*, 598−604.

(18) Kresse, G.; Hafner, J. Ab initiomolecular-dynamics simulation of the liquid-metal-amorphous-semiconductor transition in germanium. *Phys. Rev. B: Condens. Matter Mater. Phys.* **1994**, *49*, 14251−14269.

(19) Kresse, G.; Hafner, J. Ab initiomolecular dynamics for liquid metals. *Phys. Rev. B: Condens. Matter Mater. Phys.* **1993**, *47*, 558−561.

(20) Kresse, G.; Furthmüller, J. Efficient iterative schemes forab initiototal-energy calculations using a plane-wave basis set. *Phys. Rev. B: Condens. Matter Mater. Phys.* **1996**, *54*, 11169−11186.

(21) Tison, Y.; Nielsen, K.; Mowbray, D. J.; Bech, L.; Holse, C.; Calle-Vallejo, F.; Andersen, K.; Mortensen, J. J.; Jacobsen, K. W.; Nielsen, J. H. Scanning Tunneling Microscopy Evidence for the Dissociation of Carbon Monoxide on Ruthenium Steps. *J. Phys. Chem. C* **2012**, *116*, 14350−14359.

(22) Andersson, M. P.; Abild-Pedersen, F.; Remediakis, I. N.; Bligaard, T.; Jones, G.; Engbæk, J.; Lytken, O.; Horch, S.; Nielsen, J. H.; Sehested, J.; et al. Structure sensitivity of the methanation reaction: H_2-induced CO dissociation on nickel surfaces. *J. Catal.* **2008**, *255*, 6−19.

(23) Coenen, J. W. E.; van Nisselrooy, P. F. M. T.; de Croon, M. H. J. M.; van Dooren, P. F. H. A.; van Meerten, R. Z. C. The dynamics of methanation of carbon monoxide on nickel catalysts. *Appl. Catal.* **1986**, *25*, 1−8.

(24) Cheng, J.; Gong, X.; Hu, P.; Lok, C.; Ellis, P.; French, S. A Quantitative Determination of Reaction Mechanisms from Density Functional Theory Calculations: Fischer-Tropsch Synthesis on Flat and Stepped Cobalt Surfaces. *J. Catal.* **2008**, *254*, 285−295.

(25) Storsæter, S.; Chen, D.; Holmen, A. Microkinetic Modeling of the Formation of C_1 and C_2 Products in the Fischer-Tropsch Synthesis over Cobalt Catalysts. *Surf. Sci.* **2006**, *600*, 2051−2063.

(26) Cheng, J.; Hu, P.; Ellis, P.; French, S.; Kelly, G.; Lok, C. M. Chain Growth Mechanism in Fischer−Tropsch Synthesis: A DFT Study of C−C Coupling over Ru, Fe, Rh, and Re Surfaces. *J. Phys. Chem. C* **2008**, *112*, 6082−6086.

(27) Cheng, J.; Hu, P.; Ellis, P.; French, S.; Kelly, G.; Lok, C. M. An Energy Descriptor To Quantify Methane Selectivity in Fischer−

DOI: 10.1021/acs.jpcc.8b08783
J. Phys. Chem. C 2018, 122, 29249−29258

Tropsch Synthesis: A Density Functional Theory Study. *J. Phys. Chem. C* **2009**, *113*, 8858−8863.
(28) Cheng, J.; Hu, P.; Ellis, P.; French, S.; Kelly, G.; Lok, C. M. Density Functional Theory Study of Iron and Cobalt Carbides for Fischer−Tropsch Synthesis. *J. Phys. Chem. C* **2009**, *114*, 1085−1093.
(29) Kapur, N.; Hyun, J.; Shan, B.; Nicholas, J. B.; Cho, K. Ab Initio Study of CO Hydrogenation to Oxygenates on Reduced Rh Terraces and Stepped Surfaces. *J. Phys. Chem. C* **2010**, *114*, 10171−10182.
(30) de Smit, E.; Weckhuysen, B. M. The Renaissance of Iiron-Based Fischer−Tropsch Synthesis: on the Multifaceted Catalyst Deactivation Behaviour. *Chem. Soc. Rev.* **2008**, *37*, 2758−2781.
(31) Zhang, Q.; Kang, J.; Wang, Y. Development of Novel Catalysts for Fischer-Tropsch Synthesis: Tuning the Product Selectivity. *ChemCatChem* **2010**, *2*, 1030−1058.
(32) Van Der Laan, G. P.; Beenackers, A. A. C. M. Kinetics and Selectivity of the Fischer−Tropsch Synthesis: a Literature Review. *Catal. Rev.* **1999**, *41*, 255−318.
(33) Choi, Y.; Liu, P. Mechanism of Ethanol Synthesis from Syngas on Rh(111). *J. Am. Chem. Soc.* **2009**, *131*, 13054−13061.
(34) Liu, J.-X.; Su, H.-Y.; Sun, D.-P.; Zhang, B.-Y.; Li, W.-X. Crystallographic Dependence of CO activation on Cobalt Catalysts: HCP versus FCC. *J. Am. Chem. Soc.* **2013**, *135*, 16284−16287.
(35) Li, W.-Z.; Liu, J.-X.; Gu, J.; Zhou, W.; Yao, S.-Y.; Si, R.; Guo, Y.; Su, H.-Y.; Yan, C.-H.; Li, W.-X.; et al. Chemical Insights into the Design and Development of Face-Centered Cubic Ruthenium Catalysts for Fischer-Tropsch Synthesis. *J. Am. Chem. Soc.* **2017**, *139*, 2267−2276.

DOI: 10.1021/acs.jpcc.8b08783
J. Phys. Chem. C 2018, 122, 29249−29258